European Polymer Journal 141 (2020) 110099

Contents lists available at ScienceDirect

European Polymer Journal

journal homepage: www.elsevier.com/locate/europolj

Anisotropic hygro-expansion in hydrogel fibers owing to uniting 3D electrowriting and supramolecular polymer assembly

Dan Jing Wu[a,b,c], Niels H. Vonk[d], Brigitte A.G. Lamers[a,e], Miguel Castilho[f,g], Jos Malda[f,h], Johan P.M. Hoefnagels[d], Patricia Y.W. Dankers[a,b,c,*]

[a] Institute for Complex Molecular Systems, Eindhoven University of Technology, PO Box 513, 5600 MB Eindhoven, the Netherlands
[b] Laboratory of Chemical Biology, Department of Biomedical Engineering, Eindhoven University of Technology, PO Box 513, 5600 MB Eindhoven, the Netherlands
[c] Laboratory for Cell and Tissue Engineering, Department of Biomedical Engineering, Eindhoven University of Technology, PO Box 513, 5600 MB Eindhoven, the Netherlands
[d] Department of Mechanical Engineering, Eindhoven University of Technology, PO Box 513, 5600 MB Eindhoven, the Netherlands
[e] Laboratory of Macromolecular and Organic Chemistry, Department of Chemical Engineering and Chemistry, Eindhoven University of Technology, PO Box 513, 5600 MB Eindhoven, the Netherlands
[f] Department of Orthopaedics, University Medical Center Utrecht, Utrecht University, Utrecht, the Netherlands
[g] Orthopaedic Biomechanics, Department of Biomedical Engineering, Eindhoven University of Technology, PO Box 513, 5600 MB Eindhoven, the Netherlands
[h] Department of Clinical Sciences, Faculty of Veterinary Medicine, Utrecht University, Utrecht, the Netherlands

ARTICLE INFO

Keywords:
Additive manufacturing
Hydrogel
Melt electrowriting
Hygro-expansion
Supramolecular polymer

ABSTRACT

Melt electrowriting (MEW) is mostly applied to print complex three-dimensional (3D) structures using traditional, relatively hydrophobic polymers, such as polycaprolactone. Here, we 3D printed a supramolecular hydrophilic polymer into a solid micrometer-sized fiber structure, solely held together via non-covalent interactions. Interestingly, the solid fibers showed anisotropic swelling in a humid environment as demonstrated by the longitudinal and transverse surface strain determined using a novel global digital height correlation algorithm. This anisotropy in swelling is proposed to originate from a shear-induced orientation of crystals packed into lamellae as shown with small-angle x-ray scattering measurements. The MEW fibers were dried after swelling to study structural differences. Remarkably, no differences in nano-structural conformation in the micrometer-sized fibers was observed after swelling and subsequent drying. In conclusion, a free-standing supramolecular polymer-based hydrogel scaffold, displaying anisotropic hygro-expansion, is shown to be produced using MEW. This unique combination of 3D printing, via a top-down approach, and supramolecular polymer chemistry, via a bottom-up approach, provides new ways to introduce anisotropy and hierarchy in aqueous supramolecular systems. This will open the door towards even more complex hierarchical structures with unprecedented properties.

1. Introduction

Hydrogels are a class of materials often used in various biomedical applications [1–3]. These applications have been repairing and regenerating soft tissues using hydrogel scaffold matrices because of their 3D network and often (visco-)elastic properties, which are similar to the properties of native tissue. Dynamic and responsive hydrogels are promising candidates that can mimic the native extracellular matrix of tissues providing a physical environment in which cells can reside and communicate [4–7]. Synthetic supramolecular hydrogels are connected through directed non-covalent interactions, such as hydrogen bonds or electrostatic interactions to create dynamic networks, in a similar way as the self-assembly in living systems [8]. Supramolecular polymers contain extraordinary mechanical, processable, responsive, modular and tunable properties to improve the functionality of traditional biomaterials [9,10]. To form supramolecular hydrogel networks, ureidopyrimidinone (UPy) based on quadruple hydrogen bonding were telechelically coupled to poly(ethylene glycol) (PEG) chain. Consequently, these UPy-PEG polymers have shown to form supramolecular transient networks in water owing to fiber and concomitant bundle formation originating from the stacking of fourfold hydrogen bonded UPy-dimers (see Fig. 1) [11–13]. The lateral stacking into these long 1D fibers is driven by a combination of hydrophobic effects, π-π interactions and hydrogen bonding. The urea groups introduced in the hydrophobic

* Corresponding author at: Institute for Complex Molecular Systems, Eindhoven University of Technology, PO Box 513, 5600 MB Eindhoven, The Netherlands.
E-mail address: p.y.w.dankers@tue.nl (P.Y.W. Dankers).

https://doi.org/10.1016/j.eurpolymj.2020.110099
Received 30 August 2020; Received in revised form 10 October 2020; Accepted 13 October 2020
Available online 20 October 2020

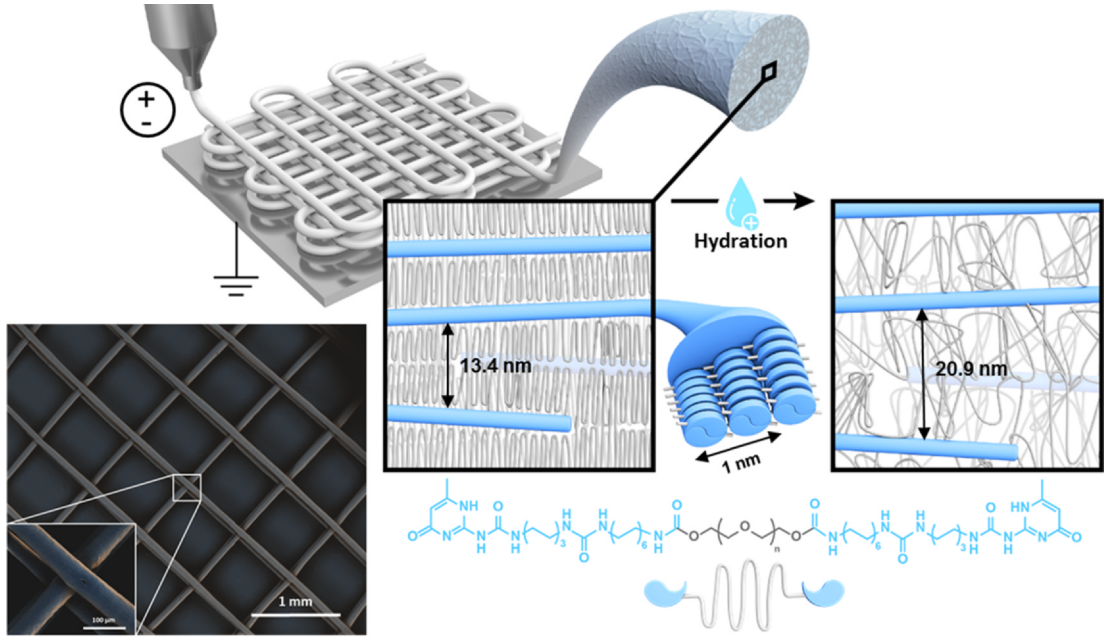

Fig. 1. Schematic illustration and scanning electron micrograph of MEW of UPy-PEG10K. Quadruple hydrogen bond formation occurs by dimerization of the UPy-moieties that form 1D stacks. Nanofibers are formed via bundling of stacks with an interstack distance of 1 nm. These UPy-moieties are telechelically connected to hydrophilic PEG polymers via hydrophobic alkyl spacers containing a urea-group to enable hydrophobic pocket formation. MEW of these UPy-PEG polymers resulted in ordered mesoscale fibrous scaffolds with segmented multiblock architectures. The lamellae phase formed by the PEG chains strengthened by hydrogen bonding in the UPy-fiber phase is 13.4 nm, measured with small angle X-ray scattering (SAXS) on dry hydrogel fibers. Exposure to water showed a reversible transition in which the fibers are anisotropically swollen owing to the ordered in nanoscale structures of lamellae phase expand to 20.9 nm. The microscopic expansion of the fiber 25.28 ± 0.04% in transverse surface strain and 4.548 ± 0.003% in longitudinal strain, as determined by GDHC measurements. Left bottom: scanning electron micrograph of MEW hydrogel scaffold.

alkyl spacer are proposed to form hydrogen bonds, and in conjunction with the alkyl spacers shield the UPy-moiety from water. The UPy-moieties and the hydrophobic spacer induce phase segregation from the polymer PEG backbone to form interstack interactions, which is the driving force for nanofiber formation. We have shown that these UPy-PEG hydrogelators can be conventionally formulated as function of hydrogelator concentration, temperature and the pH of the solution (*i.e.* the sol–gel transition occurs from basic to neutral/acidic condition) [11,12,14].

Here, we use a new methodology to create hierarchical supramolecular hydrogels from the melt into a solid scaffold using 3D printing. Subsequently, these solid UPy-PEG scaffolds are subjected to an aqueous environment to provide swelling. Various 3D printing techniques have been explored in order to produce complex mesoscale functional scaffolds [15–22]. However, the most well-established extrusion-based printing techniques are limited to resolutions of a few hundred micrometers. Recently, melt electrowriting (MEW) was introduced as a promising 3D printing technique able to create fiber scaffolds with micro- and sub-micrometer resolutions [23–25]. The electrified polymer melt is extruded by pressure and high-voltage on a computer controlled collector plate [25]. In recent years, strategies to control the electrical field during MEW has been studied in order to develop novel geometries with sub-micrometer range and desired inter-fiber spacing [26]. Tubular [27], ultrastretchable [28,29], mechanical reinforced and stabilized [30,31], multimodal and multiphasic microstructures [32–35] have been produced.

Currently, the relatively hydrophobic polymer poly(caprolactone) (PCL) is often used to produce MEW scaffolds due to ease of processing of the polymer. It remains a challenge to use hydrophilic polymers for MEW, owing to limited conductivity of the material. The dielectric constant regulates whether an electrified polymer melt is guided to the collector, which makes the printing of non-conductive materials into a controlled geometry very challenging. Additionally, hydrophilic polymers attract water from the air, which result in electric spark or repulsion during printing. Only a few examples are disclosed with the production of relatively hydrophilic scaffolds have been explored using various strategies in combination with MEW to use for hydrophilic drug encapsulation [33,36,37]. MEW of PCL blends with amphiphilic diblock copolymers consisting of poly(ethylene glycol) (PEG) and PCL segments have been tuned to fabricate hydrophilic drug loading scaffolds [37]. Post-modification of a MEW PCL scaffold with isocyanate functionalized poly(ethylene oxide-stat-propylene oxide) was used as strategy to increase hydrophilic properties to reduce unspecific protein adsorption and cell adhesion [38]. In addition, poly(2-ethyl-2-oxazoline) was used to produce hydrophilic MEW scaffolds [39].

Introduction of crosslinks using via Diels-Alder click chemistry after processing yielded scaffolds that rapidly swell in water [40].

Here, we apply MEW, via a top-down approach, and supramolecular polymer engineering, via a bottom-up approach, to develop stable and free-standing supramolecular hydrogel scaffolds. We show that these supramolecular hydrogel scaffolds anisotropically swell due to anisotropic polymer crystallization. Importantly, the swelling behavior is analyzed in detail using a novel full-field method in combination with a global digital height correlation (GDHC) algorithm [41,42]. In this way the dimensional change, *i.e.* the hygro-expansion, within a single hydrogel fiber is studied. Firstly, UPy-PEG polymers, with M_n of PEG either 10 kDa or 20 kDa (UPy-PEG_{10K}, UPy-PEG_{20K}) are processed into solid scaffolds using MEW. Characterization techniques such as differential scanning calorimetry (DSC), infrared spectroscopy (IR), gel permeation chromatography (GPC), proton-nuclear magnetic resonance (^{1}H NMR) spectrometry are performed in order to confirm no significant alteration of the material as a result of MEW. Furthermore, the structural properties at the nanometer scale within single hydrogel fibers are analyzed using small-angle x-ray scattering (SAXS) and polarized optical microscope (POM) to study the influence of the melt-extrusion based processing on the crystallization of supramolecular polymer.

2. Experimental section

2.1. Materials

The UPy-PEG polymers with $M_{n,PEG}$ = 10 kg mol^{-1} and $M_{n,PEG}$ = 20 kg mol^{-1} were synthesized by SyMO-Chem BV, Eindhoven, The Netherlands [43]. PEG polymer with $M_{n,PEG}$ = 20 kg mol^{-1} for MEW was purchased from Sigma Aldrich.

2.2. Melt electrowriting

An in-house built MEW system was used, as described previously [44]. Briefly, the system contains a high-voltage source (LNC 10000-5 pos, Heinzinger Electronic GmbH, Germany), a heating module (TR 400, HKEtec, Germany, two Nitrogen pressure regulars and a grounded computer-controlled collector plate (PMX-2EX-SA, Arcus Technology INc., USA). 500 mg of polymer was loaded and molten at 120 °C into a glass syringe and stabilized for 15 min. The syringe was flushed with nitrogen gas flow in the pressure connection before sealing the system. High voltage was used to electrify the molten hydrogel jets onto the grounded collector plate (x-y plane). To allow an homogenous hydrogel fiber collection, key instrument parameters were set to, an acceleration voltage of 3–3.5 kV, a feeding pressure of 3.0 bar and a collector velocity of 35–40 mm/s. The collector distance between the spinneret (27 G: d_I = 210 μm) and the grounded collector plate was calibrated to 3–5 mm.

2.3. Optical microscopy

Optical microscopy images of MEW materials were acquired using an Olympus SZ61 stereomicroscope coupled with an Olympus DP70 digital camera (Olympus Soft Imaging Solutions GmbH, The Netherlands). The morphology and structure of MEW UPy-PEG$_{10K}$ scaffold were further analyzed using a high-resolution scanning electron microscope (SEM; Quanta 600F, Fei, Hillsboro, OR) at high vacuum and 10 kV voltage.

2.4. Differential scanning calorimetry (DSC)

Differential scanning calorimetry (DSC) measurements were performed on a DSC Q2000 (TA instruments, USA). MEW fibers were weighed, and subsequently hermetically sealed in Tzero aluminum pans. The samples were subjected to three heating/cooling cycles from −50 °C to 180 °C with a heating/cooling rate of 10 °C min^{-1}. The melting peaks (defined as the peak maximum) and melting enthalpies (defined as the peak area) were determined from the first and second heating run using Universal Analysis software (V4.5A, TA Instruments).

2.5. Fourier transformed infrared (FTIR)

Infrared (IR) spectra were obtained on a Fourier transformed infrared spectrometer (Perkin Elmer Spectrum Two, with a Universal ATR sampling Accessory and diamond crystal, Perkin Elmer Instruments, The Netherlands) for solids. IR spectra were measured at room temperature in transmission mode with the wavelength region from 4000 to 450 cm^{-1}. UPy-PEG$_{10K}$ pristine powder and MEW fibers were positioned on the crystal and force was applied.

2.6. Gel permeation chromatography (GPC)

MEW fibers for gel permeation chromatography (GPC) were dissolved at a concentration of 1 mg mL^{-1} in dimethylformamide (DMF), supplemented with 10 mM LiBr and 0.3% (v/v) H_2O. Prior to the measurements, the sample solutions were filtered using a 0.2 μm regenerated cellulose filter. Weight-averaged molecular weights (M_w) and number-averaged molecular weights (M_n) relative to poly(ethylene glycol) standards were determined with a Varian Polymer Laboratories PL-GPC 50 Plus instrument (Varian Inc., Palo Alto, CA, USA) operated at 50 °C, equipped with a Shodex GPC KD-804 column (Shodex, Tokyo, Japan).

2.7. Proton nuclear magnetic resonance (^{1}H NMR)

^{1}H NMR spectra of the UPy-PEG$_{10K}$ powder and MEW fibers were collected on a Varian Mercury 400 MHz NMR spectrometer. Both materials were prepared in deuterated chloroform with tetramethylsilane (TMS) set as 0 ppm reference. ^{1}H NMR (400 MHz, $CDCl_3$): δ = 13.1 (2H, UPy), 11.8 (2H, UPy), 10.1 (2H, UPy), 5.9 (2H, UPy alkylidene), 4.9 (2H, urethane), 4.7 (2H, urea), 4.5 (2H, urea), 4.2 (4H, next to UPy), 3.8–3.4 (4nH, PEG), 3.2 (4H, next to urethane), 3.1 (12H, next to urethane and urea), 2.2 (6H, methyl at UPy), 1.6–1.2 (56H, hexyl and dodecyl spacer) ppm.

2.8. Full-field hygro-expansion measurement

The UPy-PEG hydrogel fibers were sprayed with polystyrene microparticles using an airbrush for tracking with the Global Digital Height Correlation (GDHC). A *Bruker NPFlex* interferometric optical profiler with 100x objective was used to obtain the fiber surface topographies, resulting in a field of view of 60 × 80 μm^2 (1376 × 1040 pixels). A climate chamber was used to control the temperature and relative humidity around the sample under the microscope. Before testing, the fibers were conditioned at room temperature and a relative humidity of 50% for 2 h. The relative humidity was increased from 50 to 90% during each testing cycle with logged relative humidity and temperature, and consecutive fiber surface topographies were captured by the optical profilometer at every ~12 s. Each fiber was tested in two relative humidity cycles.

The obtained surface topographies were processed with a GDHC algorithm dedicated to fiber swelling, which uses the minimal kinematically admissible 3D surface displacement field that fully describes the fiber swelling kinematics to correlate the topographies. This optimal kinematic regularization contains the following 6 displacement (translation and rotation) and 6 deformation (expansion and bending) modes:

- rigid body translation in the 3 principle directions (each described with a 0th-order polynomial),
- homogeneous hygroscopic expansion along 3 principle directions (1st-order polynomial),
- rotation around the 3 principle directions (1st-order polynomial)
  - o in-plane rotation (around the z-axis):

$$\vec{u} = (x(\cos(\alpha_z) - 1) - y\sin(\alpha_z))\vec{e_x} + (x\sin(\alpha_z) + y(\cos(\alpha_z) - 1))\vec{e_y}$$

  - o out-of-plane rotation (around the y-axis):

$$\vec{u} = (x(\cos(\alpha_y) - 1) - z\sin(\alpha_y))\vec{e_x} + (x\sin(\alpha_y) + z(\cos(\alpha_y) - 1))\vec{e_z}$$

  - o fiber axis rotation (around the x-axis):

$$\vec{u} = (y(\cos(\alpha_x) - 1) - z\sin(\alpha_x))\vec{e_y} + (y\sin(\alpha_x) + z(\cos(\alpha_x) - 1))\vec{e_z}$$

- small-strain approximation of bending in 3 directions (2nd-order polynomial):
  - o in-plane bending (around the z-axis):

$$\vec{u} = \kappa_z x^2 \vec{e_y} + O(x^4)$$

  - o out-of-plane bending (around the y-axis):

$$\vec{u} = \kappa_y x^2 \vec{e_z} + O(x^4)$$

  - o fiber axis bending (around the x-axis):

$$\vec{u} = \kappa_x y^2 \vec{e}_z + O(y^4)$$

with x, y and z the three principle directions and α and κ, the rotation angle and bending amplitude, respectively. The averaged strain is subsequently obtained from the strain field, resulting in the spatially-averaged longitudinal (ϵ_{ll}) and transverse surface strain (ϵ_{tt}). These surface strains were obtained for each topography measured at a certain relative humidity. Finally, the reported longitudinal and transverse strain increased (in time due to fiber swelling), and their standard deviation, were obtained by averaging over the last 100 strain data points, for which relative humidity was kept constant at 90.0 ± 0.1%.

2.9. Small angle X-ray scattering (SAXS)

Bulk small angle X-ray scattering (SAXS) was performed on SAXLAB Ganesha Lab. The flight tube and sample holder were kept under vacuum in a single housing, with a GeniX-Cu ultralow divergence X-ray generator with a wavelength (λ) of 0.154 nm and a flux of 1 × 108 ph s^{-1}. Scattered X-rays were captured on a 2-dimensional Pilatus 300 K detector with 487 × 619 pixel resolution. The sample-to-detector distance was 0.084 m (WAXS mode), 0.431 m (MAXS mode) or 1.165 m (SAXS mode). The instrument was calibrated with diffraction patterns from silver behenate.

2.10. Polarized optical microscopy (POM)

Polarized optical microscopy images (POM, Nikon) were recorded in transmission mode (dark field) with crossed polarizers and a constant polarizer angle. Post-swelling with uptake of small molecule was performed with 50 mM of nile red. 50 μL was applied on a fiber of 1.5 cm for 15 min in dark. Then, the fiber was washed 3x with ultra-pure water and images were acquired by confocal microscopy (TCS SP5X, Leica).

3. Results and discussion

3.1. Structural morphology

First, the morphology of the MEW hydrogel scaffolds was analysed using scanning electron microscopy (SEM) measurements which revealed fiber diameter of 73.9 ± 10.9 μm in the UPy-PEG_{10K} scaffolds (Fig. 1). MEW of the longer UPy-PEG_{20K} polymer did not contribute a stable jet formation as was observed when printing UPy-PEG_{10K} due to the longer PEG length resulting in the increase of hydrophilicity of the material. The MEW of non-functionalized PEG (M_n = 20 kDa) had a pulsing printing jet which resulted in droplets formation instead of reproducible fibers due to the repulsive Coulomb interactions and hydrophilicity of the material (Figure S1, Supporting Information).

All the MEW polymers (UPy-PEG_{10K}, UPy-PEG_{20K}, non-functionalized PEG) were placed into water at room temperature. The non-functionalized PEG polymer instantly dissolved in water and UPy-PEG_{20K} MEW scaffold dissolved after a few minutes while the UPy-PEG_{10K} MEW scaffold remained stable in water (Video 1, Supporting Information). Therefore, the studies on the effect of MEW processing were only conducted on the UPy-PEG_{10K} (UPy-PEG) MEW scaffolds.

3.2. Material characterization

Characterization of the printed material was performed in order to acknowledge that MEW processing technique has no influence on the molecular structure of the supramolecular materials. First, the thermal properties of the UPy-PEG before and after MEW were assessed with differential scanning calorimetry (DSC) (Table S1, Figure S2, Supporting Information). The second heating runs show no differences between the powder and fiber, *i.e.,* a melting temperature T_m of 49.6 °C with a melting enthalpy ΔH_m of 98.4 J g^{-1} for the powder, and a T_m of 51.2 °C with a ΔH_m of 97.2 J g^{-1} for the fiber, respectively. Interestingly, also the first heating runs show similar values for the T_m and ΔH_m when comparing powder with fiber. This indicates that the crystallinity in the fiber is not affected by the processing technique.

The effect of printing on the UPy-moiety was studied by the presence of various tautomeric forms of the UPy [45]. The keto-tautomer is the dominant tautomer for a UPy-moiety with a methyl on the 6-position. This keto-tautomer dimerizes into the thermodynamically most stable dimer, and forms the strong self-complementary quadruple hydrogen bonding unit. Characteristic bands in the infrared (IR) spectrum of the keto-tautomer are 1703, 1666, 1588 and 1527 cm^{-1}, which was observed in the spectrum of the pristine UPy-PEG powder (Figure S3, Supporting Information) [43]. Also, the intramolecular hydrogen bond from the pyrimidine N-H to the urea carbonyl group is present to form a centrosymmetric dimer. The bands of the hydrogen-bonded NH groups are assigned with at 2883, 2855 cm^{-1} and no free N-H vibrations were observed [46]. However, the MEW hydrogel fiber showed a small vibration around 1647, 1625 cm^{-1}, which is characteristic for the carbonyl stretch vibration of the urea group. Moreover, a slight increase of molecular mass for the MEW fibers was observed using gel permeation chromatography (GPC) (Figure S4, Supporting Information). This indicates minor crosslinking of the polymers as a result of the printing process. This result was compared with proton nuclear magnetic resonance (^{1}H NMR) measurements in order to investigate the amount and change in the chemical structure within the polymer (Figure S5, Supporting Information). An upfield of the alkylidene proton of the UPy-moiety is observed at 5.63 ppm. This proton signal indicates the presence of for 6-methylisocytosine, which corresponds to cleavage of the UPy-moiety [47]. Indication for a minor crosslinking of 9.1% within the polymers upon heating was detected with peak integration which also refers to the increased molecular mass in GPC.

After processing, the dynamic MEW UPy-PEG hydrogel scaffold was exposed to excess of water (Video 1, Supporting Information). Non-uniform swelling in the hydrogel fiberous scaffold initiate an increase in strain, which resulted in movement of the scaffold. Subsequently, a lipohilic nile red dye was dissolved into water to probe the polarity of assemblies and visualize the fibers with fluorescence microscopy. The confocal images showed the uptake of the nile red dye into the fibers during the swelling process (Fig. 2a). In this case the hydrophobic pocket of the supramolecular fibers is proposed to take up this dye, during swelling in water.[48,49] This shows that small, hydrophobic molecules can be loaded in the MEW scaffolds using a post-swelling method. Collectively, these results demonstrate the stability of of the supramolecular polymers after MEW processing and after exposing to water.

3.3. Swelling characterization with full-field method

The exact magnitude of swelling was further investigated via determination of dimensional changes of single hydrogel fibers using a novel full-field method dedicated to measure the three-dimensional surface displacement field during fiber swelling, which is an extension of the recently introduced Global Digital Height Correlation (GDHC) method [50,51]. Importantly, only 6 principle fiber deformation modes (swelling in the direction of and bending around the three principle axes) and 6 principle rigid body displacement modes (translation in the direction of and rotation around the three principle axes) are employed to correlate the evolving fiber topographies, as measured with optical profilometry (Fig. 2b). With these 12 degrees of freedom, the minimal kinematically admissible 3D surface displacement field that fully describes the fiber swelling kinematics is constituted. Use of this optimal kinematic regularization in the topography correlation yields the highest robustness and accuracy in the longitudinal (ϵ_{ll}) and transverse surface strain (ϵ_{tt}) of the hydrogel fibers (Fig. 2c). The dimensional expansion of two independent fibers was monitored while the relative humidity was increased from 50 to 90% in two cycles.

Interestingly, both fibers remain almost undeformed until a relative

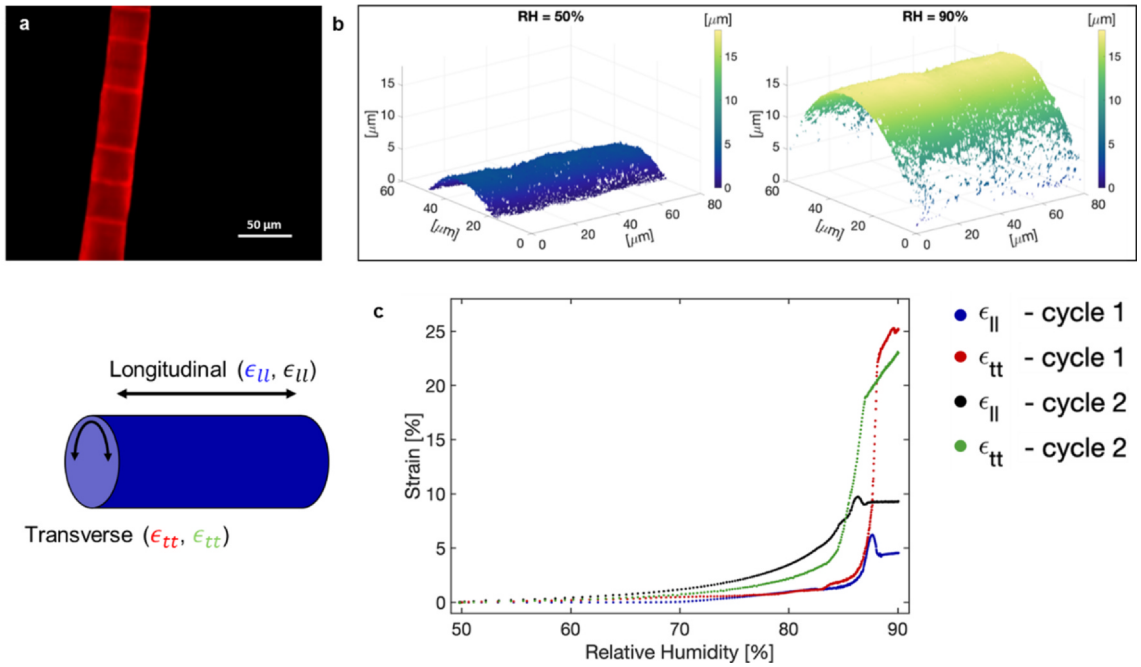

Fig. 2. Dimensional expansion of MEW hydrogel fiber and hydrogel scaffold stability. (a) Solvatochromic nile red dye staining has been used to visualize the stability of the microstructure of the hydrogel fiber after swelling. (b) Fiber topographies, obtained with optical profilometry during swelling, were correlated with a dedicated Global Digital Height Correlation algorithm to quantify the single fiber hygro-expansion. (c) The resulting surface strain in longitudinal ($_{ll}$) and transverse ($_{tt}$) direction plotted against the relative humidity (RH) for the two cycles for the hydrogel fiber. (For interpretation of the references to colour in this figure legend, the reader is referred to the web version of this article.)

humidity of approximately 85%, after which where the fibers start to expand rapidly in an anisotropic manner (Video 2 and Video 3, Supporting Information). This rapid increase saturates, for the first cycle of fiber 1, occurs at a strain of 25.28 ± 0.04% and 4.548 ± 0.003% in the transverse and longitudinal direction, corresponding to a volumetric change of 64.09% ± 0.08%. For the first cycle of fiber 2, saturation was reached at 25.14 ± 0.07% and 5.154 ± 0.005% in the transverse and longitudinal direction (Figure S6, Supporting Information) with a corresponding volumetric change of 64.67% ± 0.14%. A comparable dimensional change in transverse direction was observed for both fibers during the second cycle. With these advanced full-field measurements, the anisotropic swelling of single hydrogel fibers is confirmed, which explains the observed rotation and buckling of the fibers in the hydrogel scaffold during swelling.

3.4. Hierarchical structure analysis

In order to elucidate the molecular mechanisms at play in this hierarchically structured MEW fiber, scanning electron microscopy (SEM), polarized optical microscopy (POM) and small-angle x-ray scattering (SAXS) were employed to further probe the anisotropic swelling phenomenon. Firstly, the surface morphology of the hydrogel fiber was observed with SEM (Fig. 3a). We found a spherulitic architecture at the micrometer scale using SEM, which we attribute to shear flow-induced crystallization. It has been shown in literature that spherulites are indicative for a lamellar geometry, formed from folded chains from a nucleating center [52–54]. Moreover, POM was used to observe the alternating refractive optical property in the crystalline regions. Here, the degree of orientation was investigated by observing the extinction direction between the crossed polarizers. Birefringence was seen, which indicates that the optical axes of the domains are anisotropically orientated. This explains the macroscale anisotropic swelling behavior within the fibers, and clearly shows that molecular anisotropy translates to macroscale anisotropic behavior. The crystalline structures at 45° are shown in the optical micrographs and birefringence was observed (Fig. 3b). Hence, this result is indicative for a preferred crystallization orientation in the hydrogel fiber that is of planar fashion within the microstructures.

The orientation within the nanostructures was studied using small-angle x-ray (SAXS). A dry fiber and an overnight swollen fiber were analyzed at room temperature (Fig. 3c, d). The SAXS measurement on the dry fiber shows a primary reflection peak at $q^* = 0.47\ nm^{-1}$ with a higher order reflection at $2q^*$. These reflections are illustrative for lamellar packing (Fig. 3c). The lamellae with a domain spacing (d^*) of 13.4 nm represent the PEG phase segregated from the UPy-phase (Table S2, Supporting Information). Moreover, the PEG is crystallized, evidenced by the peaks in the wide-angle x-ray scattering (WAXS) region ($q > 10\ nm^{-1}$). A scattering peak at 6.4 nm^{-1} was observed, which can be attributed to the UPy-moiety interstack distance at 1 nm [46,55]. Furthermore, 2D medium angle scattering shows that the proposed shear stress during MEW process, induces orientation of the lamellae perpendicular to the printed fiber axis (Fig. 3c). This result is in line with the observed data using POM. Particularly, this alignment is not observed when the pristine UPy-PEG powder was melted and subsequently cooled (Fig. 3e), which indicates that the polymers undergo shear-induced orientated crystallization as the polymer jet flows through the small printing nozzle and deposit onto the collector by an electrical force and pressure. Moreover, we assume that MEW induces a more regular organization of the lamellar structure as the peak half width of the dry hydrogel fiber is significantly lower than the unprocessed powder material (Figure S7, Supporting Information). The wet hydrogel fiber was measured in a capillary with water after swelling overnight. Here, only a primary reflection peak q^* is present related to a much larger domain spacing of 20.9 nm (Fig. 3d). Most likely, this increase in domain spacing is due to the absorbance of water in the rigid lamellae packing which is known for UPy-PEG polymer in water [56]. Hence, two simultaneous events are occurring upon addition of water to the hydrogel fibers. First, the crystalline interactions of the PEG disappear, which is evidenced by the absence of sharp reflection peaks in the WAXS region. Second, the hydrophobic effect of the UPy-

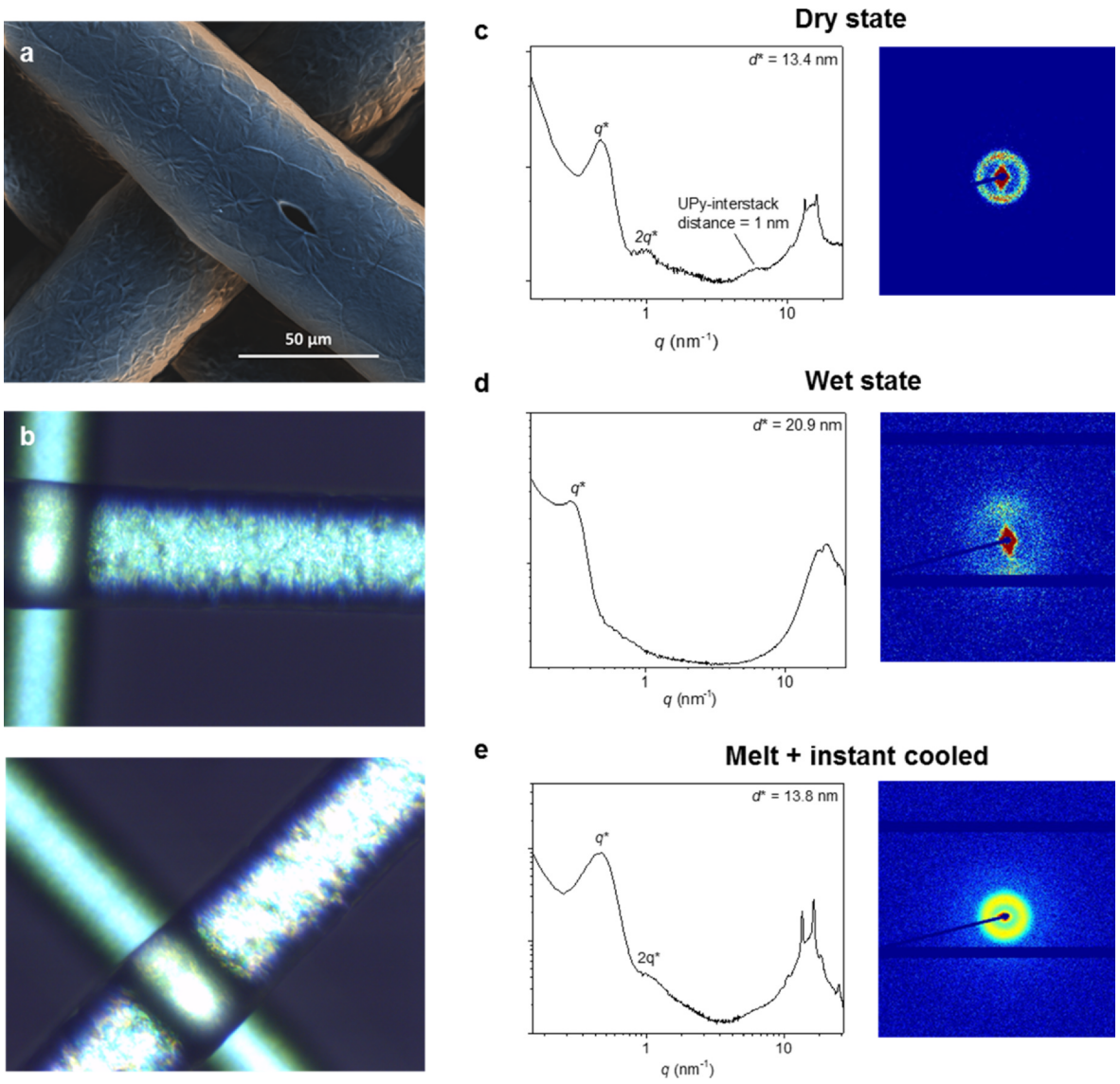

Fig. 3. Molecular alignment of the MEW hydrogel fiber induced by printing was investigated using SAXS and POM. (a) SEM image of MEW hydrogel scaffold with fine spherulitic architecture on the surface was observed. b) POM images of the scaffold after exposure to linearly polarized light at 0°- and 45°-degrees angles. Birefringent texture was observed with indication of specific orientation in the optical axes of the domains. (c,d,e) 2D medium-angle XRD of UPy-PEG were measured and Fourier transformed to 1-D data. (c) For the MEW hydrogel fiber, the propagation direction of the light during the alignment is perpendicular to the director plane. Also, lamellae packing was observed. d) After swelling of the fiber, less intense polarized light was found in the medium-angle XRD and also no lamellae packing occurs. e) For the control samples UPy-PEG melted powder, unpolarized light and scattering in all directions was observed.

moieties, in presence of water, forces stack aggregation and the amorphous PEG shield around the of UPy-moiety stacks. Hence, the larger domain spacing of the wet hydrogel fiber is a result of the phase segregation of the UPy-moiety stacks aggregated with the amorphous and flexible PEG. Interestingly, the nanostructure alignment of the material was preserved upon addition swelling in water, shown by the 2D scattering data of the wet fiber (Fig. 3d).

4. Conclusions

Here we show that a free-standing hydrophilic supramolecular polymer scaffold was successfully processed by MEW into a hierarchical hydrogel structure. The hydrogel scaffold exhibited anisotropic post-swelling behavior guided by the supramolecular orientation of the molecules in the hydrogel fiber, showing the strength of combined molecular engineering and mesoscale processing. Additionally, the hydrogel fibers are able to store hydrophobic dye molecules via post-swelling and show no loss of the morphological mesoscale fiber structure. This study opens new avenues for the design of new hierarchical hydrogel fiber scaffolds with controlled swelling behavior for different biomedical applications such as, soft robotics and shape-shifting architectures for drug delivery purposes and beyond.

CRediT authorship contribution statement

Dan Jing Wu: Conceptualization, Investigation, Validation, Formal analysis, Writing - original draft. **Niels H. Vonk:** Formal analysis, Methodology, Investigation, Writing - review & editing. **Brigitte A.G. Lamers:** Formal analysis, Methodology, Investigation, Writing - review & editing. **Miguel Castilho:** Investigation, Writing - review & editing. **Jos Malda:** Resources, Writing - review & editing. **Johan P.M. Hoefnagels:** Formal analysis, Resources, Writing - review & editing. **Patricia Y.W. Dankers:** Conceptualization, Methodology, Resources, Supervision, Project administration, Funding acquisition.

Declaration of Competing Interest

The authors declare that they have no known competing financial interests or personal relationships that could have appeared to influence the work reported in this paper.

Acknowledgement

The authors thank A.F. Mason and G. Vantomme for useful discussions on the results and the ICMS Animation Studio for careful design of the schematic representations. In addition, M. Castilho thanks the strategic alliance between University Medical Center Utrecht and Eindhoven University of Technology. This work was financially supported by the Ministry of Education, Culture and Science (Gravity programs 024.001.035 and 024.003.013).

Data availability statement

The raw/processed data required to reproduce these findings cannot be shared open access at this time as the data also forms part of a follow up study. Nevertheless, the data is accessible upon request to the authors.

Appendix A. Supplementary material

Supplementary data to this article can be found online at https://doi.org/10.1016/j.eurpolymj.2020.110099.

References

[1] J.L. Drury, D.J. Mooney, Hydrogels for tissue engineering: scaffold design variables and applications, Biomaterials 24 (2003) 4337–4351, https://doi.org/10.1016/S0142-9612(03)00340-5.
[2] A. Khademhosseini, R. Langer, Microengineered hydrogels for tissue engineering, Biomaterials 28 (2007) 5087–5092, https://doi.org/10.1016/j.biomaterials.2007.07.021.
[3] J. Li, D.J. Mooney, Designing hydrogels for controlled drug delivery, Nat. Rev. Mater. 1 (2016), https://doi.org/10.1038/natrevmats.2016.71.
[4] H.W. Ooi, C. Mota, A. Tessa Ten Cate, A. Calore, L. Moroni, M.B. Baker, Thiol-Ene alginate hydrogels as versatile bioinks for bioprinting, Biomacromolecules 19 (2018) 3390–3400, https://doi.org/10.1021/acs.biomac.8b00696.
[5] A.S. Hoffman, Hydrogels for biomedical applications, Nanostruct. Eng. Cells, Tissues Organs From Des. Appl. 64 (2018) 403–438, https://doi.org/10.1016/B978-0-12-813665-2.00011-9.
[6] H. Wang, S.C. Heilshorn, Adaptable hydrogel networks with reversible linkages for tissue engineering, Adv. Mater. 27 (2015) 3717–3736, https://doi.org/10.1002/adma.201501558.
[7] C.M. Madl, B.L. LeSavage, R.E. Dewi, K.J. Lampe, S.C. Heilshorn, Matrix remodeling enhances the differentiation capacity of neural progenitor cells in 3D hydrogels, Adv. Sci. 6 (2019), https://doi.org/10.1002/advs.201801716.
[8] G.M. Whitesides, B. Grzybowski, Self-assembly at all scales, Science (80-) 295 (2002) 2418–2421.
[9] M. Diba, S. Spaans, K. Ning, B.D. Ippel, F. Yang, B. Loomans, P.Y.W. Dankers, S.C.G. Leeuwenburgh, Self-healing biomaterials: from molecular concepts to clinical applications, Adv. Mater. Interfaces 5 (2018) 1–21, https://doi.org/10.1002/admi.201800118.
[10] T. Aida, E.W. Meijer, S.I. Stupp, Functional supramolecular polymers, Science (80-.). 335 (2012) 813–817. https://doi.org/10.1126/science.1205962.
[11] P.Y.W. Dankers, T.M. Hermans, T.W. Baughman, Y. Kamikawa, R.E. Kieltyka, M.M.C. Bastings, H.M. Janssen, N.A.J.M. Sommerdijk, A. Larsen, M.J.A. Van Luyn, A.W. Bosman, E.R. Popa, G. Fytas, E.W. Meijer, Hierarchical formation of supramolecular transient networks in water: a modular injectable delivery system, Adv. Mater. 24 (2012) 2703–2709, https://doi.org/10.1002/adma.201104072.
[12] M.M.C. Bastings, S. Koudstaal, R.E. Kieltyka, Y. Nakano, A.C.H. Pape, D.A.M. Feyen, F.J. van Slochteren, P.A. Doevendans, J.P.G. Sluijter, E.W. Meijer, S.A.J. Chamuleau, P.Y.W. Dankers, A fast pH-switchable and self-healing supramolecular hydrogel carrier for guided, local catheter injection in the infarcted myocardium, Adv. Healthc. Mater. 3 (2014) 70–78, https://doi.org/10.1002/adhm.201300076.
[13] M.J. Webber, E.A. Appel, E.W. Meijer, R. Langer, Supramolecular biomaterials, Nat. Mater. 15 (2015) 13–26, https://doi.org/10.1038/nmat4474.
[14] S.I.S. Hendrikse, S.P.W. Wijnands, R.P.M. Lafleur, M.J. Pouderoijen, H.M. Janssen, P.Y.W. Dankers, E.W. Meijer, Controlling and tuning the dynamic nature of supramolecular polymers in aqueous solutions, Chem. Commun. 53 (2017) 2279–2282, https://doi.org/10.1039/c6cc10046e.
[15] T. Jungst, W. Smolan, K. Schacht, T. Scheibel, J. Groll, Strategies and molecular design criteria for 3D printable hydrogels, Chem. Rev. 116 (2016) 1496–1539, https://doi.org/10.1021/acs.chemrev.5b00303.
[16] A. Sydney Gladman, E.A. Matsumoto, R.G. Nuzzo, L. Mahadevan, J.A. Lewis, Biomimetic 4D printing, Nat. Mater. 15 (2016) 413–418, https://doi.org/10.1038/nmat4544.
[17] K.A. Homan, D.B. Kolesky, M.A. Skylar-Scott, J. Herrmann, H. Obuobi, A. Moisan, J.A. Lewis, Bioprinting of 3D convoluted renal proximal tubules on perfusable chips, Sci. Rep. 6 (2016) 1–13, https://doi.org/10.1038/srep34845.
[18] G. Hochleitner, F. Chen, C. Blum, P.D. Dalton, B. Amsden, J. Groll, Melt electrowriting below the critical translation speed to fabricate crimped elastomer scaffolds with non-linear extension behaviour mimicking that of ligaments and tendons, Acta Biomater. 72 (2018) 110–120, https://doi.org/10.1016/j.actbio.2018.03.023.
[19] J. Malda, J. Visser, F.P. Melchels, T. Jüngst, W.E. Hennink, W.J.A. Dhert, J. Groll, D.W. Hutmacher, 25th anniversary article: engineering hydrogels for biofabrication, Adv. Mater. 25 (2013) 5011–5028, https://doi.org/10.1002/adma.201302042.
[20] C.B. Highley, C.B. Rodell, J.A. Burdick, Direct 3D printing of shear-thinning hydrogels into self-healing hydrogels, Adv. Mater. 27 (2015) 5075–5079, https://doi.org/10.1002/adma.201501234.
[21] F.P.W. Melchels, W.J.A. Dhert, D.W. Hutmacher, J. Malda, Development and characterisation of a new bioink for additive tissue manufacturing, J. Mater. Chem. B. 2 (2014) 2282–2289, https://doi.org/10.1039/c3tb21280g.
[22] A. Malheiro, P. Wieringa, C. Mota, M. Baker, L. Moroni, Patterning vasculature: the role of biofabrication to achieve an integrated multicellular ecosystem, ACS Biomater. Sci. Eng. 2 (2016) 1694–1709, https://doi.org/10.1021/acsbiomaterials.6b00269.
[23] T.D. Brown, P.D. Dalton, D.W. Hutmacher, Direct writing by way of melt electrospinning, Adv. Mater. 23 (2011) 5651–5657, https://doi.org/10.1002/adma.201103482.
[24] D.W. Hutmacher, P.D. Dalton, Melt electrospinning, Chem. – An Asian J. 6 (2011) 44–56, https://doi.org/10.1002/asia.201000436.
[25] F.M. Wunner, M.L. Wille, T.G. Noonan, O. Bas, P.D. Dalton, E.M. De-Juan-Pardo, D.W. Hutmacher, Melt electrospinning writing of highly ordered large volume scaffold architectures, Adv. Mater. 30 (2018) 1–6, https://doi.org/10.1002/adma.201706570.
[26] T.D. Brown, F. Edin, N. Detta, A.D. Skelton, D.W. Hutmacher, P.D. Dalton, Melt electrospinning of poly(ε-caprolactone) scaffolds: phenomenological observations associated with collection and direct writing, Mater. Sci. Eng. C. 45 (2015) 698–708, https://doi.org/10.1016/j.msec.2014.07.034.
[27] T.D. Brown, A. Slotosch, L. Thibaudeau, A. Taubenberger, D. Loessner, C. Vaquette, P.D. Dalton, D.W. Hutmacher, Design and fabrication of tubular scaffolds via direct writing in a melt electrospinning mode, Biointerphases 7 (2012) 1–16, https://doi.org/10.1007/s13758-011-0013-7.
[28] O. Bas, D. D'Angella, J.G. Baldwin, N.J. Castro, F.M. Wunner, N.T. Saidy, S. Kollmannsberger, A. Reali, E. Rank, E.M. De-Juan-Pardo, D.W. Hutmacher, An integrated design, material, and fabrication platform for engineering biomechanically and biologically functional soft tissues, ACS Appl. Mater. Interfaces. 9 (2017) 29430–29437, https://doi.org/10.1021/acsami.7b08617.
[29] M. Castilho, A. van Mil, M. Maher, C.H.G. Metz, G. Hochleitner, J. Groll, P.A. Doevendans, K. Ito, J.P.G. Sluijter, J. Malda, Melt electrowriting allows tailored microstructural and mechanical design of scaffolds to advance functional human myocardial tissue formation, Adv. Funct. Mater. 28 (2018) 1–10, https://doi.org/10.1002/adfm.201803151.
[30] M. De Ruijter, A. Hrynevich, J.N. Haigh, G. Hochleitner, M. Castilho, J. Groll, J. Malda, P.D. Dalton, Out-of-Plane 3D-Printed Microfibers Improve the Shear Properties of Hydrogel Composites, 1702773 (2018) 1–6. https://doi.org/10.1002/smll.201702773.
[31] M. De Ruijter, A. Ribeiro, I. Dokter, M. Castilho, J. Malda, Simultaneous Micropatterning of Fibrous Meshes and Bioinks for the Fabrication of Living Tissue Constructs, 1800418 (2019). https://doi.org/10.1002/adhm.201800418.
[32] A. Hrynevich, B. Elçi, J.N. Haigh, R. McMaster, A. Youssef, C. Blum, T. Blunk, G. Hochleitner, J. Groll, P.D. Dalton, Dimension-based design of melt electrowritten scaffolds, Small. 14 (2018) 1–6, https://doi.org/10.1002/smll.201800232.
[33] G. Hochleitner, M. Kessler, M. Schmitz, A.R. Boccaccini, J. Teβmar, J. Groll, Melt electrospinning writing of defined scaffolds using polylactide-poly(ethylene glycol) blends with 45S5 bioactive glass particles, Mater. Lett. 205 (2017) 257–260, https://doi.org/10.1016/j.matlet.2017.06.096.
[34] Y. Il Yoon, K.E. Park, S.J. Lee, W.H. Park, Fabrication of microfibrous and nano-/microfibrous scaffolds: melt and hybrid electrospinning and surface modification of poly(L-lactic acid) with plasticizer, Biomed Res. Int. (2013) 1–10, https://doi.org/10.1155/2013/309048.
[35] M. Castilho, V. Mouser, M. Chen, J. Malda, K. Ito, Bi-layered micro-fibre reinforced hydrogels for articular cartilage regeneration, Acta Biomater. 95 (2019) 297–306, https://doi.org/10.1016/j.actbio.2019.06.030.
[36] F. Chen, G. Hochleitner, T. Woodfield, J. Groll, P.D. Dalton, B.G. Amsden, Additive manufacturing of a photo-cross-linkable polymer via direct melt electrospinning writing for producing high strength structures, Biomacromolecules. 17 (2016) 208–214, https://doi.org/10.1021/acs.biomac.5b01316.
[37] N. Detta, T.D. Brown, F.K. Edin, K. Albrecht, F. Chiellini, E. Chiellini, P.D. Dalton, D.W. Hutmacher, Melt electrospinning of polycaprolactone and its blends with poly (ethylene glycol), Polym. Int. 59 (2010) 1558–1562, https://doi.org/10.1002/pi.2954.
[38] S. Bertlein, G. Hochleitner, M. Schmitz, J. Tessmar, M. Raghunath, P.D. Dalton, J. Groll, Permanent hydrophilization and generic bioactivation of melt electrowritten scaffolds, Adv. Healthc. Mater. 8 (2019) 1–8, https://doi.org/10.1002/adhm.201801544.

[39] G. Hochleitner, J.F. Hümmer, R. Luxenhofer, J. Groll, High definition fibrous poly (2-ethyl-2-oxazoline) scaffolds through melt electrospinning writing, Polymer (Guildf). 55 (2014) 5017–5023, https://doi.org/10.1016/j.polymer.2014.08.024.
[40] D. Nahm, F. Weigl, N. Schaefer, A. Sancho, A. Frank, J. Groll, C. Villmann, H.W. Schmidt, P.D. Dalton, R. Luxenhofer, A versatile biomaterial ink platform for the melt electrowriting of chemically-crosslinked hydrogels, Mater. Horizons. 7 (2020) 928–933, https://doi.org/10.1039/c9mh01654f.
[41] J. Neggers, J.P.M. Hoefnagels, F. Hild, S. Roux, M.G.D. Geers, A global digital image correlation enhanced full-field bulge test method, Procedia IUTAM. 4 (2012) 73–81, https://doi.org/10.1016/j.piutam.2012.05.009.
[42] L.I.J.C. Bergers, J. Neggers, M.G.D. Geers, J.P.M. Hoefnagels, Enhanced Global Digital Image Correlation for Accurate Measurement of Microbeam Bending, in: Springer, 2013: pp. 43–51. https://doi.org/10.1007/978-3-642-35167-9_5.
[43] P.Y.W. Dankers, E.N.M. van Leeuwen, G.M.L. van Gemert, A.J.H. Spiering, M.C. Harmsen, L.A. Brouwer, H.M. Janssen, A.W. Bosman, M.J.A. van Luyn, E.W. Meijer, Chemical and biological properties of supramolecular polymer systems based on oligocaprolactones, Biomaterials 27 (2006) 5490–5501, https://doi.org/10.1016/j.biomaterials.2006.07.011.
[44] M. Castilho, G. Hochleitner, W. Wilson, B. Van Rietbergen, P.D. Dalton, J. Groll, J. Malda, K. Ito, Mechanical behavior of a soft hydrogel reinforced with three-dimensional printed microfibre scaffolds, Sci. Rep. 8 (2018) 1–10, https://doi.org/10.1038/s41598-018-19502-y.
[45] B.B. Mollet, Y. Nakano, P.C.M.M. Magusin, A.J.H. Spiering, J.A.J.M. Vekemans, P.Y.W. Dankers, E.W. Meijer, The effect of irradiation by ultraviolet light on ureidopyrimidinone based biomaterials, J. Polym. Sci. Part A Polym. Chem. 54 (2016) 81–90, https://doi.org/10.1002/pola.27887.
[46] F.H. Beijer, R.P. Sijbesma, H. Kooijman, A.L. Spek, E.W. Meijer, Strong dimerization of ureidopyrimidones via quadruple hydrogen bonding, J. Am. Chem. Soc. 120 (1998) 6761–6769, https://doi.org/10.1021/ja974112a.
[47] B.J.B. Folmer, R.P. Sijbesma, R.M. Versteegen, J.A.J. Van Der Rijt, E.W. Meijer, Supramolecular polymer materials: chain extension of telechelic polymers using a reactive hydrogen-bonding synthon, Adv. Mater. 12 (2000) 874–878, https://doi.org/10.1002/1521-4095(200006)12:12<874::AID-ADMA874>3.0.CO;2-C.
[48] C.M.A. Leenders, L. Albertazzi, T. Mes, M.M.E. Koenigs, A.R.A. Palmans, E.W. Meijer, Supramolecular polymerization in water harnessing both hydrophobic effects and hydrogen bond formation, Chem. Commun. 49 (2013) 1963–1965, https://doi.org/10.1039/c3cc38949a.
[49] M.H. Bakker, R.E. Kieltyka, L. Albertazzi, P.Y.W. Dankers, Modular supramolecular ureidopyrimidinone polymer carriers for intracellular delivery, RSC Adv. 6 (2016) 110600–110603, https://doi.org/10.1039/C6RA22490C.
[50] J. Neggers, J.P.M. Hoefnagels, F. Hild, S. Roux, M.G.D. Geers, Direct stress-strain measurements from bulged membranes using topography image correlation, Exp. Mech. 54 (2014) 717–727, https://doi.org/10.1007/s11340-013-9832-4.
[51] S.M. Kleinendorst, J.P.M. Hoefnagels, R.C. Fleerakkers, M.P.F.H.L. van Maris, E. Cattarinuzzi, C.V. Verhoosel, M.G.D. Geers, Adaptive isogeometric digital height correlation: application to stretchable electronics, Strain. 52 (2016) 336–354, https://doi.org/10.1111/str.12189.
[52] A. Lustiger, B. Lotz, T.S. Duff, The morphology of the spherulitic surface in polyethylene, J. Polym. Sci. Part B Polym. Phys. 27 (1989) 561–579, https://doi.org/10.1002/polb.1989.090270306.
[53] K. Uchida, K. Mita, Y. Higaki, K. Kojio, A. Takahara, Lamellar orientation in isotactic polypropylene thin films: a complement study via grazing incidence X-ray diffraction and surface/cross-sectional imaging, Polym. J. 51 (2019) 183–188, https://doi.org/10.1038/s41428-018-0138-3.
[54] R.S. Graham, Understanding flow-induced crystallization in polymers: A perspective on the role of molecular simulations, J. Rheol. (N. Y. N. Y). 63 (2019) 203–214. https://doi.org/10.1122/1.5056170.
[55] W.P.J. Appel, G. Portale, E. Wisse, P.Y.W. Dankers, E.W. Meijer, Aggregation of ureido-pyrimidinone supramolecular thermoplastic elastomers into nanofibers: a kinetic analysis, Macromolecules. 44 (2011) 6776–6784, https://doi.org/10.1021/ma201303s.
[56] A.C.H. Pape, M.M.C. Bastings, R.E. Kieltyka, H.M. Wyss, I.K. Voets, E.W. Meijer, P.Y.W. Dankers, Mesoscale characterization of supramolecular transient networks using SAXS and rheology, Int. J. Mol. Sci. 15 (2014) 1096–1111, https://doi.org/10.3390/ijms15011096.